IOP Publishing Superconductor Science and Technology
Supercond. Sci. Technol. 31 (2018) 034007 (13pp) https://doi.org/10.1088/1361-6668/aaaaa6

Clean to dirty limit and T_c suppression in $NdFeAsO_{0.7}F_{0.3}$ studied by H_{c2} analysis

I Pallecchi[1,6], C Tarantini[2], Y Shen[3], R K Singh[3], N Newman[3], P Cheng[4], Y Jia[4], H-H Wen[4] and M Putti[1,5]

[1] CNR-SPIN, c/o Department of Physics, via Dodecaneso 33, 16146, Genoa, Italy
[2] National High Magnetic Field Laboratory, Florida State University, Tallahassee, FL 32310, United States of America
[3] Materials Program, Arizona State University, Tempe, AZ 85287, United States of America
[4] Institute of Physics and National Laboratory of Condensed Matter Physics, Chinese Academy of Sciences, 100190 Beijing, People's Republic of China
[5] University of Genoa, Department of Physics, via Dodecaneso 33, 16146, Genoa, Italy

E-mail: ilaria.pallecchi@spin.cnr.it

Received 18 January 2018
Accepted for publication 25 January 2018
Published 14 February 2018

Abstract

In this work, we investigate the temperature dependence of the upper critical field, dH_{c2}/dT, in an increasingly disordered $NdFeAsO_{0.7}F_{0.3}$ (NdFeAs(O,F)) single crystal that has been progressively irradiated up to a 5.25×10^{16} cm^{-2} total α-particle dose. For the $H||ab$-plane, dH_{c2}/dT does not vary remarkably with irradiation, while for the $H||c$-axis it increases sharply after the first irradiation of 3.60×10^{15} cm^{-2} and then more gradually with further irradiation doses. Focusing on the $H||c$-axis, we develop a phenomenological analysis of the H_{c2} slope which allows us to inspect the crossover from the clean to the dirty regime. From the H_{c2} slope normalized to the critical temperature and to its clean limit value, we extract the ratio of the coherence length ξ_{BCS} to the mean free path ℓ and we find that when T_c is reduced by a factor of four from its pristine value, ξ_{BCS}/ℓ becomes as large as $\sim$7 and ℓ reaches values of $\sim$1.8 nm, indicating that NdFeAs(O,F) is well into the dirty regime. Our analysis of the H_{c2} slope also allows us to compare the pair-breaking effectiveness of scattering in different superconductors, showing similarity between unconventional NdFeAs(O,F) and moderate-T_c phonon-mediated devices, such as MgB_2 and A15 compounds, but much a stronger difference with $YBa_2Cu_3O_{7-\delta}$. This work thus shows that dH_{c2}/dT is a reliable parameter, providing an alternative to residual resistivity, for investigating the pair-breaking mechanism induced by impurity scattering in superconductors.

Keywords: pair-breaking, clean and dirty limit, irradiation

(Some figures may appear in colour only in the online journal)

Introduction

The 2008 discovery of high temperature superconductivity in iron pnictides by the Hosono group [1] has offered an exceptional chance to investigate and decipher the mysteries still hidden in this phenomenon. Unconventional superconductivity, of which iron pnictides and cuprates are among the most interesting examples, refers to systems where the Cooper pairs are not bound together by phonon exchange but instead by exchange of a different kind, e.g. spin fluctuations. The signatures of unconventional superconductivity are small Fermi temperatures, superconductivity forming out of a non-Fermi liquid normal state with significant quantum critical fluctuations, existence of a pseudogap, different order parameter symmetries, and a sensitivity of the superconductor properties to impurities [2].

Among all the Fe-based compounds, iron oxypnictides REFeAsO (where RE = La, Ce, Pr, Nd, Sm, Eu, and Gd, etc) of the so called 1111 family share similar properties with cuprate superconductors. They exhibit a layered structure and a tetragonal P4/nmm space group, with a stacking series

[6] Author to whom any correspondence should be addressed.

 © 2018 IOP Publishing Ltd Printed in the UK

Table 1. Coherence length values in the *ab*-plane, $\xi_{ab}(0)$, and along the *c*-axis, $\xi_c(0)$, as estimated from the H_{c2} slope close T_c in oxypnictides of different families and in cuprates, namely YBCO and $Bi_2Sr_2CaCu_2O_x$ (BSCCO) [36].

	NdFeAs(O,F)	$Ba(FeCo)_2As_2$	Fe(Se,Te)	YBCO	BSCCO
ξ_{ab} (nm)	2.1	2.9	1.5	2.1–2.3	2.7–3.2
ξ_c (nm)	0.6	1.5	0.6	0.5–0.6	0.4–0.5

(ReO)–(FeAs)–(ReO) along the *c*-axis. FeAs forms the conducting layers, like CuO_2 in cuprates, whereas the ReO acts as blocking layers. In the parent compounds Fe is ordered antiferromagnetically, as Cu is in cuprates. As a consequence of these similarities, their superconducting properties exhibit similar characteristics. Oxypnictides exhibit the highest critical temperature T_c among the iron-based superconductors, reaching 58 K in SmFeAs(F,O) [3] (without external pressure). Its upper critical fields are extremely high [4–6] and anisotropic [7–9]. The shape of the resistive transition is significantly broadened by the magnetic field [5, 7, 9], which is reminiscent of the behavior of the high-T_c cuprates. $\mu_0 dH_{c2}/dT$ close to T_c are around $-10\,T\,K^{-1}$ and $-2\,T\,K^{-1}$ for H parallel and perpendicular to the *ab*-plane, respectively [7–10], and are slightly larger than those reported for the $YBa_2Cu_3O_{7-\delta}$ (YBCO) family [11–13]. The H_{c2} anisotropy is ~7–5 close to T_c [7–9, 14] and is then found to slightly decrease with declining temperature. These anisotropy values, representative of optimally doped compounds, are on average similar to those reported for the YBCO family and much lower than those of the Bi-based compounds. Going from the optimally doped to the underdoped regime, H_{c2} progressively decreases in F doped SmFeAsO compounds [15], whereas in cuprates it systematically increases [16]. This discrepancy may reflect the different nature of the ground state of the parent compounds in pnictides and cuprates; the former being uncompensated metals while the latter are Mott insulators. The large H_{c2} values are a consequence of short coherence lengths both in cuprates and in pnictides. We report low temperature limits of the coherence length in the *ab*-plane, $\xi_{ab}(0)$, and along the *c*-axis, $\xi_c(0)$, in table 1. Clearly they are very similar in NdFeAsO and YBCO. In the case of cuprates it was argued that these small values could prevent the crossover from the clean to the dirty limit, which occurs when the mean free path becomes smaller than the coherence length [17]. Reaching the dirty limit has important implications for the superconducting properties, both beneficially and detrimentally, as H_{c2} is enhanced due to the decrease of the effective Ginzburg–Landau coherence length, ξ_{GL}, but at the same time T_c is progressively suppressed due to pair-breaking impurity scattering in the dirty limit. These aspects have been extensively investigated in disordered cuprate superconductors [17–20].

In addition to the implication of the crossover from the clean to the dirty limits on the superconducting properties, the relationship between pair-breaking impurity scattering and T_c suppression is a fundamental one. This has been addressed in a number of momentous theoretical works, starting in the late 1950s [21–25]. It is well known that T_c is insensitive to non-magnetic impurity scattering in a single-band isotropic s-wave superconductor, as long as disorder does not appreciably affect the density of states [21, 22], and magnetic impurity scattering suppresses T_c according to the Abrikosov-Gor'kov law [26–28]. On the other hand, superconductors with different gap symmetries or anisotropic gaps [29] may be extremely sensitive even to non-magnetic impurities. Representative examples thereof are the odd order parameter superconductors, such as d-wave high-T_c cuprates [22] and $s^{\pm}$ wave iron pnictides [30]. Moreover, in multigap superconductors, even with s-wave symmetry, similarly to the case of anisotropic superconductors, a sizeable T_c suppression by non-magnetic *interband* scattering is predicted by theory [24], and this behavior is indeed observed in MgB_2 [31, 32].

Within this variegated scenario, with several unknown microscopic parameters and unavoidable simplifying assumptions necessary to extract parameters from the experimental data [33], the theoretical prediction of the rate of T_c suppression and its comparison with experiments is not straightforward. In particular, the roles of microscopic parameters such as gap structures, types of scattering defects, inter- to intraband scattering ratios, and multiband parameters, are critical [33, 34].

Irradiation with energetic particles (electrons, protons, neutrons, α-particles, and heavy ions) is an effective way to systematically introduce defects and study the relationship between impurity scattering and T_c suppression, with minimal impact on material parameters such as chemical potential and band structure. Different types of defects are produced in iron pnictides by irradiation with increasing particle mass and energy, from point-like Frenkel pairs, to clusters of point-like defects, to columnar tracks [35].

In this paper we address the relationship between impurity scattering and superconducting properties in an increasingly α-particle irradiated oxypnicide $NdFeAsO_{0.7}F_{0.3}$ (NdFeAs(O,F)) single crystal, initially in the clean limit and eventually reaching the dirty limit. We investigate whether the analysis of the slope of the upper critical field, dH_{c2}/dT, can be used as a tool to evaluate the role of impurity scattering on the superconducting properties, as an alternative to the more usual analyses of residual resistivity, which presents some limitations. On the other hand, similarly to the analysis of residual resistivity, also the analysis of the slope of the upper critical field in oxypnicide superconductors should require taking into account the multiband character, the wave-function symmetry, and the type of impurity scattering potential. In fact, in multiband superconductors the extraction of a single scattering rate from experiments (as done in the analyses of residual resistivity) is a simplifying assumption that does not actually provide the relevant pair-breaking scattering rate, which is the *interband* component of the scattering rate. However, this multiband framework should rely on a large number of fitting parameters, which could be

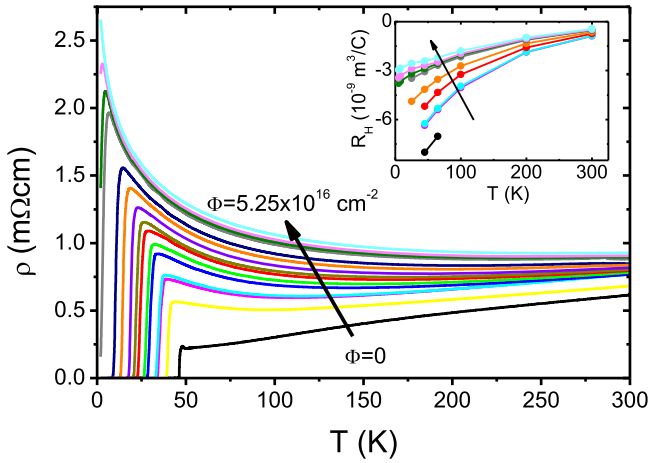

Figure 1. Resistivity (main panel) and Hall resistance (inset) measured in the pristine sample (black curve) and at different irradiation levels. Increasing irradiation dose Φ is indicated by the arrows. The same color legend identifying the dose level is maintained in the main panel and inset.

hardly determined univocally, even in the fortunate case that complete $H_{c2}(T)$ curves are available. Hence, herein we explore the possibility of carrying out a simplified *effective phenomenological* analysis that assesses the overall effect of disorder on superconducting properties, parametrized by the mean free path, and also allows direct comparison between different superconductors. We can thereby discuss our results in comparison to the case of YBCO, and also with reference to conventional superconductors that are interesting for applications, such as the MgB_2 and A15 compounds.

Experimental details

The α-particle irradiation was performed on a $NdFeAsO_{0.7}F_{0.3}$ single crystal [37], where Pt contacts for resistivity and Hall measurements were prepared using a focused ion beam. The thickness of the sample was about 1 μm, the distance between the voltage contacts was ~13 μm and T_c before irradiation was 46.4 K (estimated at the 90% of the extrapolated normal-state resistance). The α-particle irradiation was carried out with a 2 MeV $^4He^{2+}$ ion beam from a tandem accelerator at 300 K. The sample was irradiated in 14 steps up to a total dose of $5.25 \times 10^{16}/cm^2$. The magnetoresistence as a function of temperature was measured up to 9 T after each irradiation step using a Quantum Design Physical Property Measurement System. Simulations using the Stopping and Range of Ions in Matter-2008 software show that the mean free path of $^4He^{2+}$ ions in $NdFeAsO_{0.7}F_{0.3}$ is about 4.2 μm, which ensures uniform radiation damage throughout the sample thickness. The collisions occur mainly on the Nd, Fe, and As sites, while the effect on O/F sites is minor.

Experimental results

Figure 1 shows the resistivity curves $\rho(T)$ after each irradiation step. In the inset, the Hall resistance R_H curves measured for a subset of irradiation doses are also shown. T_c decreases monotonically after each irradiation step without significant broadening of the resistivity transition. Superconductivity is completely suppressed after an accumulated dose of $5.25 \times 10^{16}/cm^2$. The normal-state resistivity progressively increases after each irradiation dose with a significant upturn developing at low T. The logarithmic trend of low T resistivity as a function of temperature was attributed to the Kondo effect due to magnetic scattering with uncompensated moment of displaced Fe and Nd atoms [37].

Magnetoresistance was measured after each irradiation step, with the magnetic field applied parallel and perpendicular to the c-axis. The results obtained after the fourth irradiation step are reported in figure 2. The resistive transitions are shifted to lower temperature with increasing field, without significant broadening in comparison with those observed in the crystal before irradiation [5]. The reduced vortex dissipation in the applied magnetic field could be partly due to the lower T_c and to the increased pinning as a consequences of irradiation.

The H_{c2} values are estimated at 90% of the normal-state resistance, taking into account the normal-state logarithmic behavior. The values calculated after each irradiation step for H parallel to the c-axis and to the ab-plane are reported in figures 3(a) and (b), respectively. The H_{c2} curves shift towards low temperature with a slight steady change of slope with increasing irradiation. Similar behavior of nearly parallel H_{c2} curves was observed in a neutron irradiated LaFeAs(O,F) polycrystalline sample [38], first heavily irradiated in order to completely suppress T_c and then annealed to heal the damage from irradiation. The slopes dH_{c2}/dT are evaluated by a linear fit of $H_{c2}(T)$ curves, excluding the low field ($H < 1$ T) data that exhibit upward curvature, while the error bars on these values are estimated by further linear fitting of the same data, either excluding a larger range of low field data points ($H < 2$ T) or including all data points. These slopes $\mu_0 dH_{c2}/dT$ are plotted versus T_c, evaluated at the 90% of the normal-state resistance, in figure 4. The slopes of our pristine sample are -7.3 T K^{-1} and -1.3 T K^{-1} for the $H||ab$-plane and $H||c$-axis, respectively. For the $H||ab$-plane, the H_{c2} slope changes smoothly and weakly with irradiation, whereas for the $H||c$-axis the slope increases more visibly after the first irradiation step and then it increases slowly in further steps. Indeed the anisotropy γ_{Hc2} defined as the ratio of $H||ab$ to $H||c$, drops from 5.6 to 3.1 after the first dose and then smoothly decreases and becomes about 2.4 when T_c is about to be completely suppressed (see the inset of figure 4). This fact that γ_{Hc2} does not reach unity at high disorder is different from what was observed in irradiated anisotropic superconductors such as MgB_2 [39]. Indeed, usually the strong disorder suppressing T_c increases the coherence length ξ_{GL}, which eventually becomes much larger than the lattice parameters, thus driving the system towards the isotropic limit. In the following we focus our analysis on the dH_{c2}/dT values for the field direction $H||c$-axis.

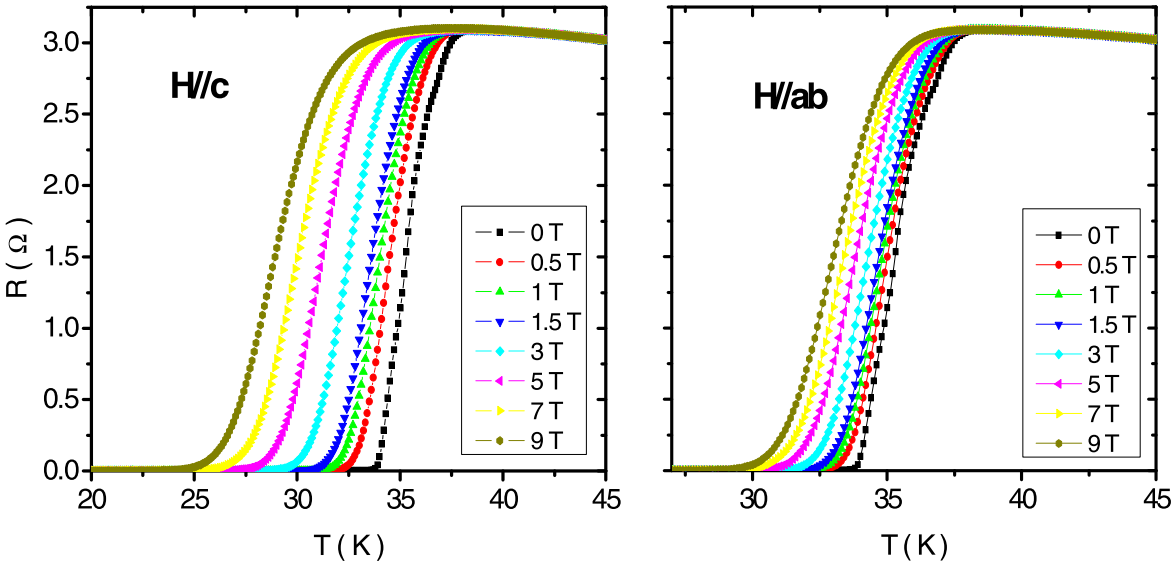

Figure 2. Resistance measured after the fourth irradiation step in magnetic fields up to 9 T, applied parallel (left) and perpendicular (right) to the *c*-axis. The selected data are typical and represent any irradiation step.

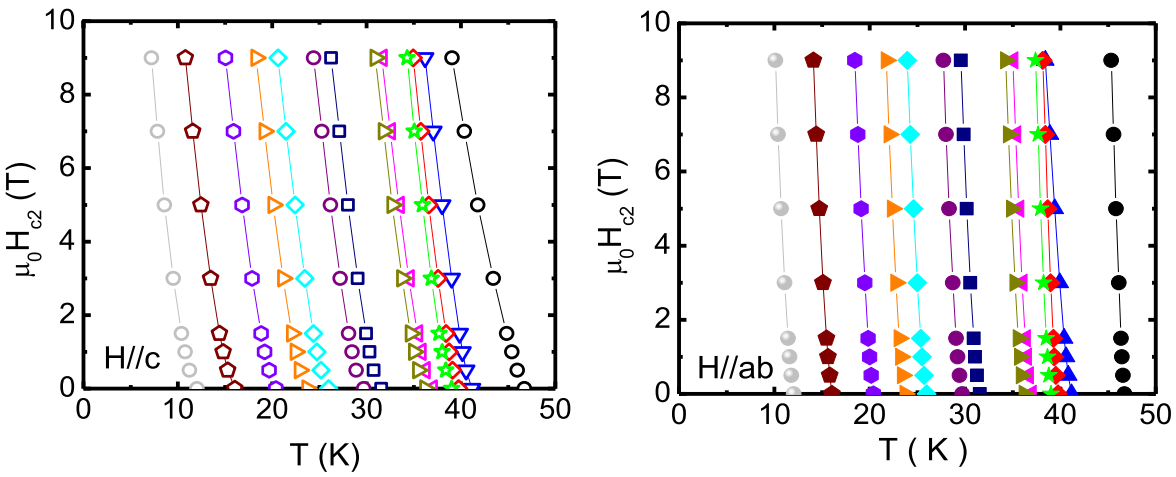

Figure 3. H_{c2} curves measured after each irradiation step with H parallel (left) and perpendicular (right) to the *c*-axis.

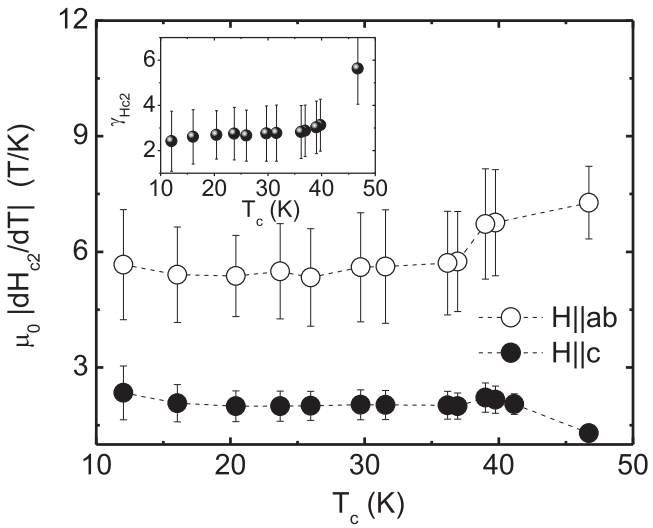

Figure 4. Upper critical field slopes dH_{c2}/dT as a function of T_c. Inset: anisotropy γ_{Hc2} as a function of T_c.

Phenomenological background: the effect of impurity scattering on H_{c2}

We aim to compare the dependence of the H_{c2} slope and T_c on the irradiation defects in NdFeAs(O,F) with that observed on other technical superconductors, namely YBCO, MgB , and Nb_3Sn in order to assess the tendency to reach the dirty limit and the robustness to disorder. These superconductors have deeply different natures in terms of conventional versus unconventional pairing, isotropic versus anisotropic superconducting properties, and multiband versus single-band behavior. In each case, suitable theoretical frameworks have been developed to take into account these aspects, yet a simplified scenario describing the overall effect of disorder on superconducting properties could allow direct comparison between these different superconductors. In this section we summarize some relevant equations that describe the dependence of the H_{c2} slope and T_c on disorder and propose a set of phenomenological effective equations by which we can

analyse and compare the experimental data measured on different superconductors.

Starting from the clean limit, with increasing scattering from defects, the upper critical field H_{c2} increases [40] and its slope dH_{c2}/dT close to T_c can be written as [17, 41]:

$$|dH_{c2}/dT| \approx \eta \frac{T_c}{\langle v_F^{*2} \rangle}(1 + \lambda_{tr}). \quad (1)$$

Indeed, in the absence of scattering, the clean limit slope of the upper critical field, dH_{c2}/dT, is determined by the quantity $\eta T_c / \langle v_F^{*2} \rangle$ [42, 43], where for a strong-coupled superconductor $\langle v_F^{*2} \rangle = \langle (v_F/(1 + \lambda))^2 \rangle$ is the Fermi surface-averaged squared Fermi velocity, renormalized by the coupling constant λ, and η, the strong-coupling correction factor for the upper critical field, representing the ratio of the strong-coupling pair-breaking to the corresponding weak-coupling BCS counterpart [41, 44, 45]. According to equation (1), with increasing scattering, the clean limit dH_{c2}/dT is corrected by an additional term proportional to λ_{tr}, the transport coupling constant, which increases with decreasing mean free path ℓ or decreasing transport scattering time $\tau = \ell / v_F^*$, being defined as [17]

$$\lambda_{tr} = \frac{\hbar}{2\pi k_B T_c \tau^*} = 0.882 \frac{\xi_{BCS}}{\ell} \quad (2)$$

where $\hbar$ is the Planck constant, k_B the Boltzmann constant, and $\xi_{BCS} = 0.18\hbar v^*/k_B T_c$ the zero temperature limit of the BCS coherence length. In the above expression, $\tau^* = \tau(1 + \lambda)$ and $v_F^* = v_F/(1 + \lambda)$ are the renormalized scattering time and Fermi velocity. We define the reduced H_{c2} slope, equation (1) divided by T_c, as follows:

$$\left| \frac{1}{T_c} \frac{dH_{c2}}{dT} \right| \approx \eta \frac{1}{\langle v_F^{*2} \rangle}(1 + \lambda_{tr}). \quad (3)$$

As long as the defects do not affect the electronic structure appreciably, the variation of $\eta / \langle v_F^{*2} \rangle$ with increasing disorder can be neglected and its clean limit ($\lambda_{tr} \ll 1$) value $\left. \frac{\eta}{\langle v_F^{*2} \rangle} \right|_{\lambda_{tr}=0} = \frac{1}{T_{c0}} \frac{dH_{c20}}{dT}$ can be assumed (here the 0 subscript in H_{c2} and T_c indicates the pristine clean limit values). Thus equations (2) and (3) can be combined to write:

$$\left| \frac{1}{T_c} \frac{dH_{c2}}{dT} \right| = \left| \frac{1}{T_{c0}} \frac{dH_{c20}}{dT} \right| (1 + \lambda_{tr}) = \left| \frac{1}{T_{c0}} \frac{dH_{c20}}{dT} \right| \left(1 + 0.882 \frac{\xi_{BCS}}{\ell} \right). \quad (4)$$

Equation (4) provides a convenient way to inspect the clean to dirty limit crossover on the superconductor properties by analysing the behavior of the reduced H_{c2} slope normalized to its pristine clean limit value. Indeed, the normalized H_{c2} slope is expected to remain virtually constant and equal to its clean limit dH_{c20}/dT as long as $\xi_{BCS}/\ell \ll 1$, while it should increase in magnitude with decreasing mean free path as the ξ_{BCS}/ℓ ratio becomes comparable or larger than unity.

The quantity λ_{tr} also measures the rate of T_c suppression by pair-breaking. Indeed different models which consider odd symmetry order parameters, anisotropic gap superconductors, and multiband superconductors [22, 29, 33] for low disorder and small T_c suppression $\lambda_{tr} \ll 1$ (or $T_c \tau \gg \hbar/(2\pi k_B)$) [22, 29], yield an approximate relationship of the type

$$T_c = \frac{T_{c0}}{1 + \alpha \lambda_{tr}} \quad (5)$$

where T_{c0} is the pristine clean limit value of the transition temperature and α is a numeric parameter proportional to the pair-breaking effectiveness of scattering by impurities.

Using equation (2), equation (5) can be rewritten as [46]:

$$\frac{T_{c0}}{T_c} = 1 + \alpha \lambda_{tr} = 1 + \alpha 0.882 \frac{\xi_{BCS}}{\ell}. \quad (6)$$

Now, by comparing equation (4) and equation (6), it appears that both the $\left| \frac{1}{T_c} \frac{dH_{c2}}{dT} \right|$ enhancement and T_c suppression depend on the same ratio $\lambda_{tr} = 0.882\ \xi_{BCS}/\ell$, so that:

$$\left(\frac{1}{T_c} \frac{dH_{c2}}{dT} \Big/ \frac{1}{T_{c0}} \frac{dH_{c20}}{dT} \right) - 1 = \lambda_{tr} \quad (7.a)$$

$$(T_{c0}/T_c) - 1 = \alpha \lambda_{tr}. \quad (7.b)$$

The quantities dH_{c2}/dT and T_c are both easily measurable in our experiment and can be used to extract the parameter α defined by equation (5), whose value is a measure of the T_c suppression rate by scattering. Specifically, the slope of the linear regime at low disorder in the plot of

$$(T_{c0}/T_c) - 1 \quad \text{versus} \quad \left(\frac{1}{T_c} \frac{dH_{c2}}{dT} \Big/ \frac{1}{T_{c0}} \frac{dH_{c20}}{dT} \right) - 1 \quad (8)$$

gives directly the α parameter.

We finally note that the quantity λ_{tr} is related to the dimensionless pair-breaking parameter g usually introduced to measure the pair-breaking effect [24, 47]. This pair-breaking parameter is defined as $g = \Gamma\hbar/4\pi k_B T_{c0}$, where $\Gamma = 1/\tau$ is the scattering rate. Considering that $\xi_{BCS} = 0.18\hbar v^*/k_B T_c$ and $\tau^* = \ell/v_F^*$, the relationship between λ_{tr} and g is easily obtained as

$$g = \frac{\Gamma^* \hbar}{4\pi k_B T_{c0}} = \frac{v_F^* \hbar}{4\pi \ell k_B T_{c0}} = \frac{v_F^* \hbar}{k_B T_c} \frac{T_c}{T_{c0}} \frac{1}{4\pi\ell} = \frac{\xi_{BCS}}{0.18} \frac{T_c}{T_{c0}} \frac{1}{4\pi\ell} \approx 0.44 \frac{\xi_{BCS}}{\ell} \frac{T_c}{T_{c0}}. \quad (9)$$

Data analysis

Analysis of H_{c2} slope with increasing disorder

Comparison between different superconductors. We start our analysis by considering the behavior of the upper critical field in NdFeAs(O,F) with increasing disorder, in comparison with other superconductors. In particular, we consider literature data on electron irradiated YBCO films [19], α-particle and neutron irradiated MgB_2 films [39, 48], and ion irradiated Nb_3Sn films [49]. In MgB_2 the multigap/multiband behavior is pretty marked, due to the peculiarly different nature of the σ or the

π bands in terms of symmetry, anisotropy, coupling with phonons, and sign of charge carriers. As a consequence, in MgB_2 H_{c2} is mainly related to the parameters of either the σ or the π band, depending on the dirty or clean limit and on the temperature range [50, 51]. Thus, for this case, tailored multiband data analysis is required. Yet, in the following, we disregard this aspect and compare the overall trends of H_{c2} in the different superconductors. Also, the different types of irradiation used for the data collected and compared in this section—electrons, neutrons, α-particles, and ions—produce different types of defects. The particle mass and energy determine the attenuation length and the recoil energy, which in turn may result in either uniformly distributed point defects, or additional correlated disorder and extended defects such as clusters and cascades of point defects and even, in the extreme case, columnar tracks. MeV-range electron irradiation is characterized by long attenuation lengths on the scale of the sample size and small recoil energy, thus producing point defects in the form of vacancy-interstitial (Frenkel) pairs [35]. On the other hand, heavier particles such as protons, neutrons, and α-particles also generate correlated disorder [52]. Specifically, such particles mainly generate uniform point-like defects by collisions on atomic sites along their path, while larger size defects with inhomogeneous distribution are produced at the end of their range [53]. For 2 MeV α-particles, such as those used in this experiment, a range longer than the sample thickness has been evaluated, which ensures uniform irradiation damage throughout the sample, caused by collisions on the Nd, Fe, and As sites, with minor effects on O/F sites. In our analysis we focus on the effect of disorder on H_{c2}, which is mainly sensitive to the point-like disorder that limits the mean free path, regardless of the additional presence of correlated disorder. Hence we compare the different data sets on an equal footing.

In the left panel of figure 5, we plot the H_{c2} slope versus increasing disorder, measured by the ratio T_{c0}/T_c. According to equation (1), since with increasing disorder λ_{tr} as a consequence of the decreasing mean free path ℓ, T_c decreases (see equation (5)) and the non-monotonic behavior of dH_{c2}/dT is determined at low levels of disorder by the increased λ_{tr}, followed by a decrease at higher levels of disorder where the effect of the T_c suppression becomes dominant. If we divide dH_{c2}/dT by the respective T_c, we can focus on just the increase of the H_{c2} slope due the decrease of the mean free path, as indeed can be observed in the right panel of figure 5. However, we must not forget that with increasing disorder, the density of states may be significantly altered from its pristine value, as widely observed and modeled in the case of A15 compounds [45, 54–56], yielding an additional decrease of the H_{c2} slope at high disorder. Indeed, in Nb_3Sn, for an almost completely suppressed T_c from its pristine value, a decrease of the density of states by 30% has been estimated [55]. Also, for MgB_2 a 20% reduction in the density of states by this mechanism is proposed to almost completely eliminate the T_c [57, 58]. On the other hand, in the cases of NdFeAs(O,F) and YBCO it is reasonable to assume that any effect of suppression of the density of states by disorder is mild, due to the smoother

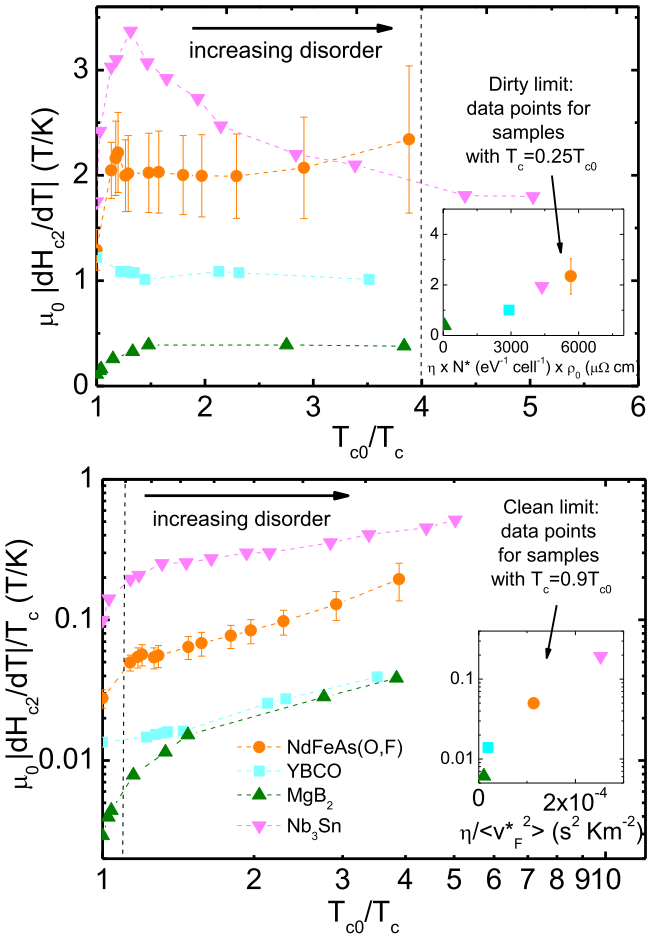

Figure 5. $\mu_0 dH_{c2}/dT$ (top) and $(\mu_0 dH_{c2}/dT)/T_c$ (bottom) as a function of increasing disorder measured by the ratio T_{c0}/T_c for our α-particle irradiated NdFeAs(O,F) crystal compared to the same quantity measured in electron irradiated YBCO films [19], α-particle and neutron irradiated MgB_2 films [39, 48], and ion irradiated Nb_3Sn films [49]. In the inset of the top panel, $\mu_0 dH_{c2}/dT$ is plotted versus the product of resistivity and density of states for data points in the heavily dirty limit ($T_{c0}/T_c = 4$, that is $T_c = 0.25T_{c0}$, indicated by a vertical dashed line in the main panel). In the inset of the bottom panel, the $(\mu_0 dH_{c2}/dT)/T_c$ is plotted versus the inverse squared Fermi velocity for data points close to the clean limit ($T_{c0}/T_c = 1.1$, that is $T_c = 0.9T_{c0}$, indicated by a vertical dashed line in the main panel). The symbol legend is common to both panels and both insets. The vertical axes of the insets report the same quantity as the vertical axes of the respective main panels.

features of the density of states as a function of energy close to the Fermi level in NdFeAs(O,F) [59] and YBCO [60] when compared to A15 compounds and MgB_2.

As for the comparison of the magnitude of H_{c2} slope in different superconductors, we note that in the heavily dirty limit ($\lambda_{tr} \gg 1$), equation (1) yields $|dH_{c2}/dT| \approx \eta \frac{T_c}{\langle v_F^{*2} \rangle} \lambda_{tr}$, which can be rewritten as

$$|dH_{c2}/dT| \approx \eta \frac{T_c}{\langle v^{*2} \rangle} \lambda_{tr} \propto \eta \rho N^* \quad \text{for} \quad \lambda_{tr} \gg 1 \qquad (10)$$

where ρ is the low temperature normal-state residual resistivity and $N^* = N(1 + \lambda)$ is the renormalized density of electronic states at the Fermi level E_F [61], possibly

affected by disorder. Equation (10) is obtained using the approximation $\lambda_{tr} \propto \frac{\xi_{BCS}}{\ell} \propto \frac{v^*}{\ell T_c} = \frac{v^*}{v^* \tau^* T_c} \propto \frac{\rho n}{T_c m}$, $n \approx N^* E_F$, and $mv^{*2} \propto E_F$, where n is the carrier concentration and m the carrier effective mass. Hence, if we consider the dirty limit data points ($T_{c0}/T_c \approx 4$, or equivalently $T_c \approx 0.25T_{c0}$) in the left panel of figure 5, as well as the respective resistivity values taken from each reference, the calculated densities of states N [41, 45, 55, 58–60, 62–64], the coupling constants λ [41, 55, 64–66], and the strong-coupling corrections factors η [6, 41, 67, 68] taken from the literature, as reported in table 2, we find a proportionality relationship between $|dH_{c2}/dT|$ and the product $\eta\rho N^*$, as demonstrated in the inset of the left panel of figure 5.

A further check on the comparison of the magnitude of H_{c2} slope in different superconductors can be carried out on the data of dH_{c2}/dT normalized to T_c (right panel of figure 5), considering the low disorder limit ($\lambda_{tr} \ll 1$), where equation (3) yields:

$$\left| \frac{1}{T_c} \frac{dH_{c2}}{dT} \right| \approx \frac{\eta}{\langle v_F^{*2} \rangle} \quad \text{for } \lambda_{tr} \ll 1. \tag{11}$$

Hence, if we consider data points close to the clean limit ($T_{c0}/T_c \approx 1.1$, or equivalently $T_c \approx 0.9T_{c0}$) in the right panel of figure 5, as well as Fermi velocity values taken from the literature and reported in table 2 [45, 55, 58, 69–72], we find a proportionality relationship between $\left| \frac{1}{T_c} \frac{dH_{c2}}{dT} \right|$ and $\eta/\langle v_F{}^{*2} \rangle$, as demonstrated in the inset therein.

Given the approximated character of equations (1), (10), and (11), the large uncertainty on the estimation of Fermi velocity, coupling constant, strong-coupling corrections factors, and density of states values, the fact that we have used the rough approximation $\langle v_F^{*2} \rangle \approx \langle v_F^* \rangle^2$, the proportionality plots shown in the two insets of figure 5, representing the dirty and clean limits respectively, are remarkable.

Crossover from the clean to the dirty limit. The above phenomenological laws correctly describe the trend in dH_{c2}/dT for different superconductors in both the dirty and clean limits, indicating that the H_{c2} analysis is a reliable tool to investigate the effect of disorder, once material specific parameters related to electronic band structure and coupling are taken into account. Hence, in the following we go further into the analysis of our irradiated NdFeAs(O,F) sample, to extract quantitative information on the mean free path and coherence length.

We start our analysis by using equation (4). In figure 6, we plot the reduced dH_{c2}/dT normalized to its clean limit value versus T_c/T_{c0}. As T_c departs from T_{c0}, the data points depart from unity and the amount of this departure is just a measure of $\lambda_{tr} = 0.882\ \xi_{BCS}/\ell$, going from the clean to the dirty limit (right to left in figure 6). It is seen that, as T_c is reduced to 85% of its pristine value, the mean free path becomes equal to ξ_{BCS}, $\xi_{BCS}/\ell \approx 1$, and, as T_c is further reduced to 25% of its pristine value, ℓ becomes almost seven times smaller than ξ_{BCS}, which is indicative of being deep in the dirty limit. For comparison, data measured in electron irradiated YBCO films taken from [19] are also plotted in the same graph. In this plot, we limit our comparison to YBCO, because in the case of MgB_2 the multiband nature dramatically influences the behavior of dH_{c2}/dT as a function of both temperature and disorder, while in the A15 compounds the suppression of the density of states contributes to the behavior of the dH_{c2}/dT together with the decrease in the mean free path. Remarkably, it can be observed that for similar T_c suppression, approaching the dirty limit due to the decreasing mean free path is about four times slower in YBCO compared to NdFeAs(O,F). Indeed in YBCO a T_c drop to 25% of its pristine value corresponds to an ℓ that is 2.4 times smaller than ξ_{BCS}. This indicates that disorder is much more effective in suppressing superconductivity in YBCO than in NdFeAs(O,F). From the data in figure 6, we can also directly access the value of the mean free path by considering that, according to the expression $\xi_{BCS} = 0.18\hbar v^*/KT_c$, the clean limit coherence lengths ($\xi_{ab} \approx 2.1$ nm for both NdFeAs(O,F) and YBCO, see table 1) change as $1/T_c$, as long as the electronic structure is not appreciably affected by disorder, and thus neither is v_F. In table 3, we list the calculated mean free paths ℓ for given T_c/T_{c0} ratios. It turns out that for NdFeAs(O,F), ℓ is suppressed down to 1.2 nm for $T_c/T_{c0} = 0.25$, while in YBCO, ℓ is still as large as 3.4 nm for the same T_c suppression. This confirms the larger effectiveness of disorder in suppressing superconductivity in YBCO than in NdFeAs (O,F). Incidentally, we note that the values for NdFeAs(O,F) are in agreement with those found using the Drude model to determine the mean free path ℓ_{Drude} from resistivity and Hall effect measurements ($\ell_{Drude} = 1.5$ nm for $T_c/T_{c0} = 0.5$ and $\ell_{Drude} = 1.2$ nm for $T_c/T_{c0} = 0.25$, while for $T_c = T_{c0}$ $\ell_{Drude} = 6.9$ nm).

Hence this analysis evidences that disorder in pnictides allows us to reach the dirty limit while not suppressing the critical temperature too much. This provides two beneficial effects, both important for applications, namely the increase of the upper critical field and the decrease of the H_{c2} anisotropy γ_{Hc2}, as reported in figure 4. We note that the anisotropy is reduced, but not fully removed even down to the lowest T_c. This can be understood considering the Ginzburg–Landau length ξ_{GL}, whose values are reported in table 3. In the clean limit ξ_{GL} coincides with ξ_{BCS}, while in the dirty limit $\xi_{GL} \approx \sqrt{\xi_{BCS}\ell}$. With decreasing T_c, given the huge reduction of the mean free path ℓ, ξ_{GL} is only weakly increased, so that the ratio ξ_{GL}/γ_{Hc2} does not largely exceed the c-axis lattice parameter, which is the condition to remove the anisotropy.

Analysis of T_c versus disorder

Comparison between different superconductors. According to equation (7.a), the normalized ratio $\frac{1}{T_c}\frac{dH_{c2}}{dT}$ just gives λ_{tr}, which measures the effectiveness of disorder in carrying the system in the dirty limit. This parameter λ_{tr} also appears in equation (6), which allows us to evaluate the effectiveness of

Table 2. Parameters of different superconducting compounds: clean limit transition temperature T_{c0}, density of states, Fermi velocity, coupling constants, strong-coupling correction factors, low temperature normal-state residual resistivity for a sample with $T_c = 0.25T_{c0}$, slopes of the upper critical field for samples with $T_c = 0.25T_{c0}$, slopes of the upper critical field divided by T_c for samples with $T_c = 0.9T_{c0}$. The source references are in square parentheses.

	T_{c0} (K)	Density of states (eV^{-1} $cell^{-1}$)	v_F (km s^{-1})	λ	η	ρ for sample with $T_c = 0.25T_{c0}$ ($\mu\Omega$ cm)	$\mu_0 \left\lvert \frac{dH_{c2}}{dT} \right\rvert$ for sample with $T_c = 0.25T_{c0}$ (T K^{-1})	$\mu_0 \left\lvert \frac{1}{T_c}\frac{dH_{c2}}{dT} \right\rvert$ for sample with T_c=$0.9T_{c0}$ (T K^{-1})
NdFeAs (O,F)	46	4 [59] [a]	160 [71] [a]	0.6 [65] [a]	1.14 [6]	775 [[37], this work]	3.28 [this work]	0.051 [this work]
YBCO	92	0.75 [60]	250 (exp) [69, 70] [b]	2.6 [66]	1.2 [67, 68]	900 [73]	1.0 [19]	0.014 [19]
MgB_2	39	0.71 [63, 69]	490 [58] [c]	0.5 [64] [c]	1 [c]	55 [39, 48, 58]	0.39 [39, 48, 58]	0.0061 [39, 48, 58]
Nb_3Sn	18	10 [45, 55] [d]	210 [45, 55]	1.8 [41, 55]	1.42 [41]	110 [49, 58]	1.94 [49, 58]	0.19 [49, 58]

[a] The density of states and Fermi velocity data are calculated for LaFeAsO (La-1111) rather than NdFeAs(O,F), but it has been shown that all REFeAsO (RE = rare earth) exhibit pretty similar band structures [74]. The average Fermi velocity of holes and electrons bands of La-1111 is considered. Also the coupling constant extracted from optical measurements is for La-1111.

[b] This value of Fermi velocity for YBCO is extracted from experiments (angle resolved photoemission spectroscopy), hence it represents $v_F^* = v_F/(1 + \lambda)$, rather than the bare v_F as for all the other theoretical estimations reported in this table.

[c] An average value between calculated Fermi velocities and coupling constants of σ and π bands is used here. For the coupling correction factor we assume $\eta \approx 1$, as MgB_2 is well described in the BCS framework. On the other hand, by taking an average value of the two gaps [75], $\eta \approx 1$ is indeed obtained.

[d] For Nb_3Sn, the density of states predicted for a disordered sample having resistivity $\rho \approx 100$ $\mu\Omega$ cm and $T_c = 0.25T_{c0}$ is considered here, because it is known that in A15 compounds the density of states is suppressed by disorder [56, 58].

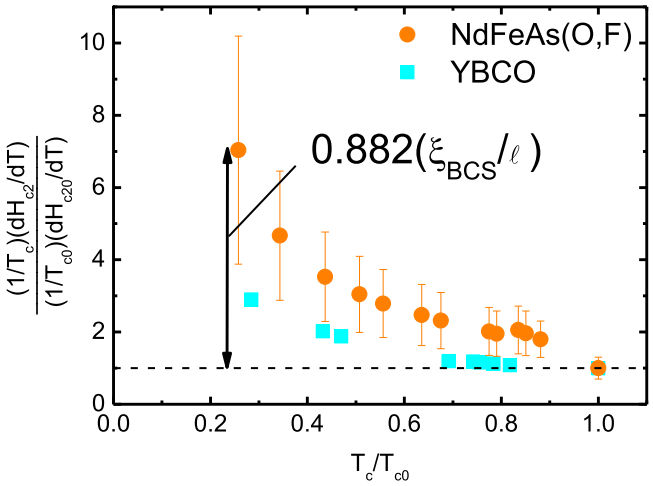

Figure 6. H_{c2} slope normalized to the critical temperature and to its clean limit value versus T_c/T_{c0}, plotted for our α-particle irradiated NdFeAs(O,F) and for electron irradiated YBCO films taken from [19].

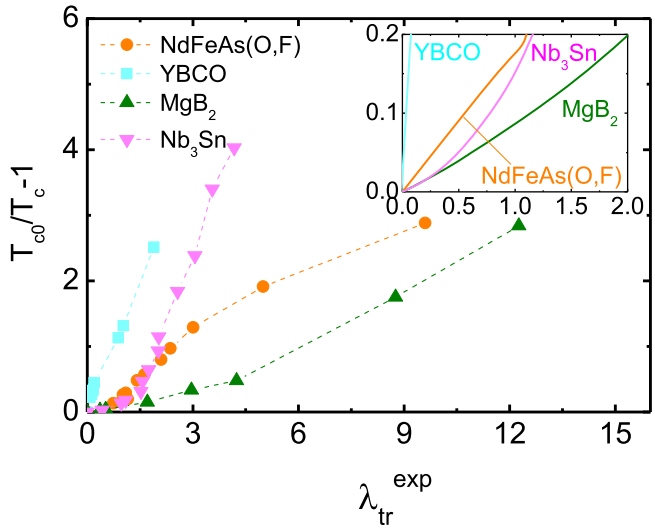

Figure 7. T_{c0}/T_c with unity offset plotted as a function of $(dH_{c2}/dT)/T_c$ normalized to its clean limit value and with unity offset as well, for our α-particle irradiated NdFeAs(O,F), as compared electron irradiated YBCO films [19], α-particle and neutron irradiated MgB_2 films [39, 48], and ion irradiated Nb_3Sn films [49]. In the inset, the linear behavior in the low $(T_{c0}/T_c - 1)$ regime is magnified.

Table 3. Values of ξ_{BCS}, mean free path ℓ, and ξ_{GL} in NdFeAs(O,F) and YBCO for different T_c suppression from T_{c0}, extracted from data in figure 6.

	NdFeAs(O,F)			YBCO		
T_c/T_{c0}	ξ_{BCS} (nm)	ℓ (nm)	ξ_{GL} (nm)	ξ_{BCS} (nm)	ℓ (nm)	ξ_{GL} (nm)
1	2.1	$\gg$2.1	2.1	2.1	$\gg$2.1	2.1
0.5	4.2	1.8	2.8	4.2	5.1	4.6
0.25	8.4	1.2	3.2	8.4	3.4	5.3

Table 4. Parameter α, defined by equation (5), which quantifies the pair-breaking effectiveness of scattering, extracted from the data of figure 7.

Samples	α-parameter
α-particle irradiated NdFeAs(O,F) crystal	0.18
electron irradiated YBCO films	2.2
α-particle and neutron irradiated MgB_2 films	0.09
ion irradiated Nb_3Sn films	0.15

scattering as a pair-breaking process. Therefore, we can infer an experimental estimation of λ_{tr} from the analysis of H_{c2} as $\lambda_{tr}^{exp} = \left[\left(\frac{1}{T_c}\frac{dH_{c2}}{dT} \Big/ \frac{1}{T_{c0}}\frac{dH_{c20}}{dT}\right) - 1\right]$. In figure 7, we plot $(T_{c0}/T_c) - 1$ versus λ_{tr}^{exp}, as indicated by equation (8), for the same set of samples as in figure 5. In the inset, it is clearly observed that in the low disorder regime, i.e. $[(T_{c0}/T_c) - 1] < 0.2$, all the curves are almost linear. Hence, according to equation (8), from the linear slopes we can directly determine the numeric parameter α, as defined by equation (5), whose magnitude is proportional to the pair-breaking effectiveness of scattering. In table 4, we report the extracted α values for the different superconductors. Similar values are obtained for conventional Nb_3Sn and MgB_2 and NdFeAs(O,F), while a much larger value is extracted for YBCO. From theory, the α value is expected to be vanishing in single-band s-wave superconductors for non-magnetic scattering, and non-vanishing for d-wave superconductors and multiband s^{++} and $s^{\pm}$ wave superconductors with interband scattering [24]. The superconductors considered here belong to all the categories, Nb_3Sn being s-wave single-band, MgB_2 s-wave two-band (s^{++}), and YBCO d-wave; in the case of iron pnictides, two types of symmetries (s^{++} and $s^{\pm}$) have been proposed. Our results show that for Nb_3Sn, despite its single-band s-wave nature, α is not negligible and comparable with two-band MgB_2. The sensitivity of A15 compounds to impurities was explained by the smearing of the density of states caused by disorder [45]; while in MgB_2 the main ingredient is the interband scattering between σ and π bands, which causes the merging of the energy gaps [24, 57]. Thus, the similar behavior of Nb_3Sn and MgB_2 with respect to impurity is probably a coincidence, as reported and discussed in [58]. The large α values obtained for YBCO is in agreement with expectation, given the odd symmetry of the order parameter in cuprate superconductors [76]. Quantitatively, NdFeAs(O,F) is closer to conventional superconductors than to YBCO. This finding is consistent with other experimental results in the literature [77–79] which assess the robustness of T_c in iron-based superconductors against disorder. This results should be discussed in terms of pairing symmetry.

The $s^{\pm}$ symmetry associated to interband interactions between hole and electron pockets mediated by spin fluctuations, which lead to a superconducting order parameter that changes sign over the Fermi surface sheets, is most often used to describe iron pnictides. The theoretical consequences are found to be consistent with most experiments that investigate the role of pair-breaking effect by impurities [46]. Indeed, despite earlier experiments [77, 80–82] claiming

that the rate of T_c suppression by disorder was much slower than what predicted by the $s^{\pm}$ scenario [83], later theoretical works dealing with multiband $s^{\pm}$ superconductivity considered different types of impurity scattering potentials (finite-ranged potential, different ratios of interband to intraband contributions…) and demonstrated that results for the $s^{\pm}$ state are not inconsistent with experimental data. Remarkably, for $s^{\pm}$ symmetry, intraband scattering does not suppress T_c (according to Anderson's theorem [22]), whereas interband scattering does, hence by adjusting the ratio of intraband to interband scattering, the experimental rate of T_c suppression is reproduced by theory [34, 84, 85]. The alternative s^{++} wave description proposed for iron pnictides, based on interband interactions mediated by charge fluctuations, does not imply any sign reversal across Fermi surface sheets and should correspond to a small influence of pair-breaking by impurities on the superconductor properties [83], as observed in some experiments [86].

Comparison between different routes to extract the pair-breaking parameter. Combining equations (2), (7.a), and (9), the pair-breaking parameter g can be extracted from the H_{c2} slope as:

$$g^{(H_{c2})} \approx 0.5\left[\left(\frac{1}{T_c}\frac{dH_{c2}}{dT}\Big/\frac{1}{T_{c0}}\frac{dH_{c20}}{dT}\right)-1\right]\frac{T_c}{T_{c0}}. \qquad (12)$$

On the other hand, the same pair-breaking parameter is usually extracted from residual resistivity data [19, 37, 46], once the scattering rate is obtained from either Hall effect data, first principles calculations, or London penetration depth λ_{pd} values [77, 81]. The results of these three different routes differ by a factor 2–3 from one another in iron pnictides [77, 81]. Usually the latter route is preferred, as it avoids direct estimation of carrier density and effective mass, hence the g parameter is calculated as

$$g^{(\rho-\lambda_{pd})} = \frac{\hbar}{2\pi k_B \mu_0}\frac{\Delta\rho_0}{T_{c0}{\lambda_{pd}}^2} \approx 0.24\frac{\Delta\rho_0[\mu\Omega\mathrm{cm}]}{T_{c0}[\mathrm{K}]} \qquad (13)$$

where μ_0 is the vacuum magnetic permeability, $\Delta\rho_0$ is the disorder-induced variation of the residual resistivity from its clean limit, and the numeric factor takes into account the value of the London penetration depth $\lambda_{pd} \approx 200$ nm measured in pnictide compounds of different families [87–89]. In the main panel of figure 8, we display the T_c/T_{c0} versus g plot for a collection of literature data on irradiated pnictide superconductors. In all cases, the g values are extracted from resistivity data using the London penetration depth values. Clearly, the curves are spread over a wide range, as also evidenced in the review of [46]. This spread may be explained by the different compounds, different types of irradiation, different doping levels, different pristine T_{c0}, magnetic or non-magnetic scattering. Regarding the latter issue, however, almost equal T_c suppression rates with magnetic (e.g. Mn substitution in the Fe site) and non-magnetic impurities are found experimentally [90]. In addition to the mentioned reasons for the observed spread, it is likely that in most cases also a correct estimation of $\Delta\rho_0$ is affected by such factors as uncertainties in geometrical factors, grain boundary contributions, the Kondo effect, and localization mechanisms. This makes it worth considering alternative experimental probes of impurity scattering, for example the H_{c2} slope.

In the inset of figure 8, the curve extracted in this work from the H_{c2} slope analysis is directly compared with the T_c/T_{c0} versus g plot obtained from the residual resistivity analysis carried out on the same sample, in [37]. The departure between the two curves is significant and may be explained by considering the limitations of both residual resistivity and H_{c2} slope as experimental probes of disorder in multiband superconductors. The residual resistivity is determined by the parallel of the residual resistivities of the two bands and thus it mainly reflects the properties of the cleaner band, thus underestimating the introduced disorder. On the other hand, H_{c2} reflects the properties of the band with the larger H_{c2}, which is the dirtier one. Yet, as recalled in the previous section, only the disorder associated with *interband* scattering has a pair-breaking effect in multiband superconductors, while both the analyses of residual resistivity or H_{c2} slope generally rely on a single scattering rate extracted from the experiment. Hence, it turns out that, with this simplifying assumption, both the analyses of resistivity and the H_{c2} slope can only provide qualitative plots of T_c/T_{c0} versus g for any multiband superconductor. It is worth noting that the comparison of the T_c/T_{c0} versus g plots obtained from the H_{c2} slope and resistivity analyses has also been carried out in cuprates, which are free of multiband complications, and indeed the agreement was found to be satisfying [19].

Conclusions

We study the evolution of the upper critical field slope dH_{c2}/dT in an increasingly disordered oxypnicide crystal, namely a $NdFeAsO_{0.7}F_{0.3}$ single crystal progressively irradiated with α-particles, with the goal of visualizing the crossover from the clean to the dirty limit, and gaining information on the pair-breaking effect of impurity scattering. The proposed phenomenological analysis of the H_{c2} slope, already applied to high-T_c cuprates [19], relies on effective parameters, neglecting the multiband nature and the symmetry of the order parameter in NdFeAs(O,F). Such simplification is, on one hand, a limit, but on the other hand it circumvents the problem of a larger number of fitting multiband parameters, which would be undetermined by the available experimental data, just consisting of a set of linear slopes of H_{c2} close to T_c. Moreover, this phenomenological effective approach—which fulfils the expected scaling for different superconducting compounds, of either conventional or unconventional character, both in clean and dirty regimes—can be used to directly compare the behavior of such superconductors.

Focusing on the configuration $H||c$-axis, from the reduced H_{c2} slope normalized to its clean limit value, we

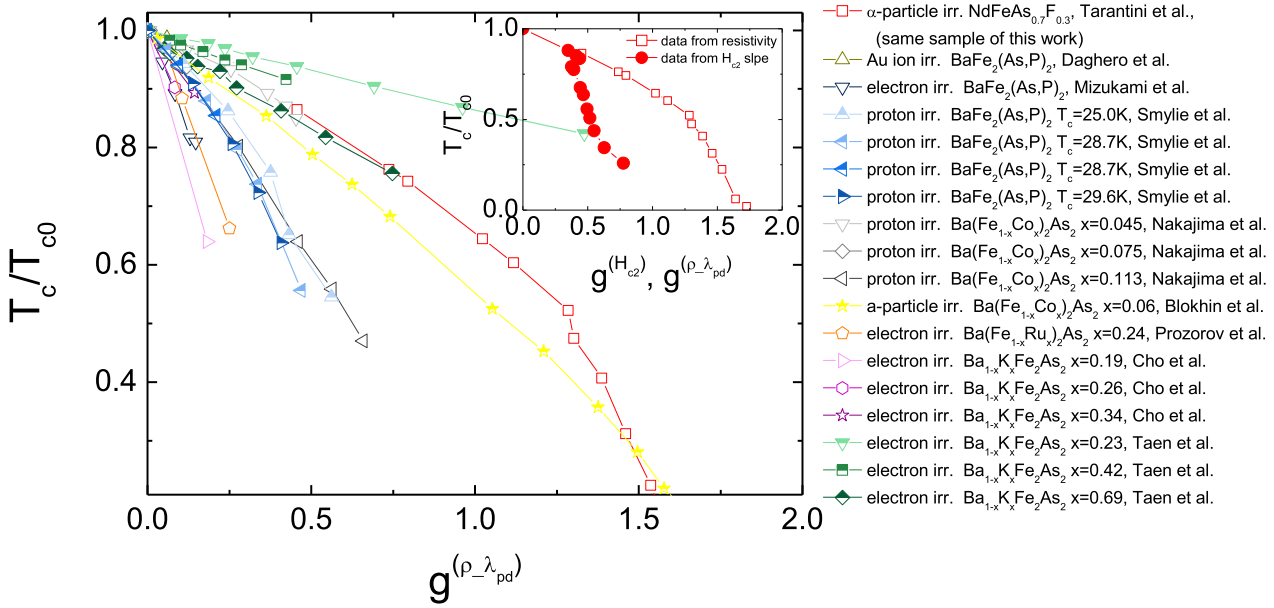

Figure 8. T_c/T_{c0} versus pair-breaking factor g calculated by equation (13) from residual resistivity data for the NdFeAs(O,F) sample of this work [37] and for other irradiated superconducting iron pnictides from the literature, namely, Au ion irradiated Au ion irradiated $BaFe_2(As,P)_2$ [91], electron irradiated $BaFe_2(As,P)_2$ [35], proton irradiated $BaFe_2(As,P)_2$ with different T_c [92], proton irradiated $Ba(Fe_{1-x}Co_x)_2As_2$ with different doping levels [77], α-particle irradiated $Ba(Fe_{1-x}Co_x)_2As_2$ with $x = 0.06$ [93], electron irradiated $Ba(Fe_{1-x}Ru_x)_2As_2$ with $x= 0.24$ [33], electron irradiated $Ba_{1-x}K_xFe_2As_2$ with different doping levels [81, 94]. Inset: comparison of the T_c/T_{c0} versus pair-breaking factor g curve obtained in this work for the NdFeAs(O,F) sample from the H_{c2} slope using equation (12), with the same curve obtained from residual resistivity data using equation (13) on the same sample [37].

extract the ratio of the coherence length to the mean free path ξ_{BCS}/ℓ in our NdFeAs(O,F) crystal. For T_c reduced by a factor of four from its pristine value, ξ_{BCS}/ℓ becomes as large as $\sim$7 and ℓ reaches values of $\approx$1.8 nm. This suggests that in NdFeAs(O,F) the strongly dirty regime can be attained before superconductivity is completely suppressed. Remarkably, the approach to the dirty limit resulting from the decreasing mean free path is about four times slower in YBCO compared to NdFeAs(O,F) for similar T_c suppression. Judging from further analyses of dH_{c2}/dT data, the influence of scattering on pair-breaking is comparable in NdFeAs(O,F) and in conventional superconductors such as MgB_2 and A15 compounds, but stronger in YBCO.

Our phenomenological analysis is not adequate to make quantitative comparisons with theoretical models in order to obtain information on the pairing symmetry in pnictides. Indeed, for multiband superconductors, extracting a single pair-breaking parameter from either resistivity data or H_{c2} slope data does not allow to evaluate the interband component of the scattering rate, which is mostly responsible for the suppression of superconductivity. Yet, qualitative information obtained from our analysis is a powerful tool to compare the pair-breaking effect of disorder and the crossover from the clean to the dirty limit in superconductors of different nature. In this respect, it is desirable that more experimental H_{c2} data on series of increasingly disordered superconducting samples, together with resistivity data, are made available in the literature, to shed further light on the role of the multiple parameters into play.

In conclusion, our analysis has reached the goal of assessing the effect of disorder on the superconducting properties of a NdFeAs(O,F) sample. Our findings show that in pnictides it is possible to introduce disorder that increases the upper critical fields, decreases the anisotropy, and at the same time does not suppress the critical temperature too much. This feature, joined with the large value of the critical temperature itself, makes these compounds interesting for many applications.

Acknowledgments

The authors are grateful to Alex Gurevich and David Larbalestier for scientific discussions.

Financial support from the Italian Ministry for Research through the PRIN project RIDEIRON (contract n. 2012X3YFZ2) is acknowledged.

ORCID iDs

I Pallecchi https://orcid.org/0000-0001-6819-6124
C Tarantini https://orcid.org/0000-0002-3314-5906

References

[1] Kamihara Y, Watanabe T, Hirano M and Hosono H 2008 *J. Am. Chem. Soc.* **130** 3296
[2] Stewart G R 2017 *Adv. Phys.* **66** 75–196
[3] Fujioka M *et al* 2013 *Supercond. Sci. Technol.* **26** 085023

[4] Hunte F, Jaroszynski J, Gurevich A, Larbalestier D C, Jin R, Sefat A S, McGuire M A, Sales B C, Christen D K and Mandrus D 2008 *Nature* **453** 903
[5] Jaroszynski J *et al* 2008 *Phys. Rev.* B **78** 064511
[6] Fuchs G *et al* 2008 *Phys. Rev. Lett.* **101** 237003
[7] Jaroszynski J *et al* 2008 *Phys. Rev.* B **78** 174523
[8] Lee H-S, Bartkowiak M, Park J-H, Lee J-Y, Kim J-Y, Sung N-H, Cho B K, Jung C-U, Kim J S and Lee H-J 2009 *Phys. Rev.* B **80** 144512
[9] Putti M *et al* 2010 *Supercond. Sci. Technol.* **23** 034003
[10] Jia Y, Cheng P, Fang L, Luo H, Yang H, Ren C, Shan L, Gu C and Wena H-H 2008 *Appl. Phys. Lett.* **93** 032503
[11] Tajima Y *et al Phys. Rev.* B **37** 79561988
[12] Zimmermann P *et al Phys. Rev.* B **52** 5411995
[13] Welp U, Kwok W K, Crabtree G W, Vandervoort K G and Liu J Z 1989 *Phys. Rev. Lett.* **62** 1908
[14] Weyeneth S, Puzniak R, Zhigadlo N D, Katrych S, Bukowski Z, Karpinski J and Keller H 2009 *J. Supercond. Nov. Magn.* **22** 347–51
[15] Pallecchi I, Fanciulli C, Tropeano M, Palenzona A, Ferretti M, Malagoli A, Martinelli A, Sheikin I, Putti M and Ferdeghini C 2009 *Phys. Rev.* B **79** 104515
[16] Wang Y, Ono S, Onose Y, Gu G, Ando Y, Tokura Y, Uchida S and Ong N P 2003 *Science* **299** 86
[17] Shabanova N P, Krasnosvobodtsev S I, Varlashkin A V and Golovashkin A I 2002 *Phys. Solid State* **44** 1840
[18] Krasnosvobodtsev S I, Shabanova N P, Nozdrin V S and Golovashkin A I 1999 *Phys. Solid State* **41** 1256
[19] Lin J-Y, Chen S J, Chen S Y, Chang C F, Yang H D, Tolpygo S K, Gurvitch M, Hsu Y Y and Ku H C 1999 *Phys. Rev.* B **59** 6047
[20] Weber H W 1986 *Irradiation Damage in Superconductors* (*Advances in Cryogenic Engineering Materials* vol 32) (New York: Plenum) ch 102 pp 853–64
[21] Anderson P W 1959 Theory of dirty superconductors *J. Phys. Chem. Solids Suppl.* **11** 26
[22] Anderson P W 1961 *Phys. Rev.* **124** 41
[23] Abrikosov A A 2000 *Physica* C **341-348** 97–102
[24] Golubov A A and Mazin I I 1997 *Phys. Rev.* B **55** 15146
[25] Anderson P W 1959 *J. Phys. Chem. Solids* **11** 26
[26] Abrikosov A A and Gor'kov L P 1960 Theory of superconducting alloys with paramagnetic impurities *Zh. Eksp. Teor. Fiz.* **39** 1781
Abrikosov A A and Gor'kov L P 1961 Contribution to the theory of superconducting alloys with paramagnetic impurities *Sov. Phys. JETP* **12** 1243
[27] Balatsky A V, Vekhter I and Zhu J-X 2006 *Rev. Mod. Phys.* **78** 373
[28] Samokhin K V 2012 Effects of impurities in non-centrosymmetric superconductors *Non-Centrosymmetric Superconductors* (Lecture Notes in Physics) vol 847 (Berlin: Springer) pp 269–95
[29] Abrikosov A A 1993 *Physica* C **214** 107
[30] Hirschfeld P J, Korshunov M M and Mazin I I 2011 *Rep. Prog. Phys.* **74** 124508
[31] Gandikota R *et al* 2005 *Appl. Phys. Lett.* **86** 012508
[32] Putti M, Affronte M, Ferdeghini C, Manfrinetti P, Tarantini C and Lehmann E 2006 *Phys. Rev. Lett.* **96** 077003
[33] Prozorov R, Konczykowski M, Tanatar M A, Thaler A, Bud'ko S L, Canfield P C, Mishra V and Hirschfeld P J 2014 *Phys. Rev.* X **4** 041032
[34] Wang Y, Kreisel A, Hirschfeld P J and Mishra V 2013 *Phys. Rev.* B **87** 094504
[35] Mizukami Y *et al* 2014 *Nat. Commun.* **5** 5657
[36] Pallecchi I and Putti M 2015 Iron-based superconductors: materials aspects for applications *Handbook of Applied Superconductivity* ed P Seidel (Weinheim: Wiley) ch 2.2.2 pp 166–91
[37] Tarantini C *et al* 2010 *Phys. Rev. Lett.* **104** 087002
[38] Karkin A E, Werner J, Behr G and Goshchitskii B N 2009 *Phys. Rev.* B **80** 174512
[39] Gandikota R *et al* 2005 *Appl. Phys. Lett.* **87** 072507
[40] Werthamer N R (ed) 1969 *Superconductivity* vol 1 ed R D Parks (New York: Marcel Dekker) p 321
[41] Orlando T P, McNiff E J Jr, Foner S and Beasley M R 1979 *Phys. Rev.* B **19** 4545
[42] Gor'kov L P and Melik-Barkhudarov T K 1963 *Zh. Éksp. Teor. Fiz.* **45** 1493
Gor'kov L P and Melik-Barkhudarov T K 1964 *Sov. Phys. JETP* **18** 1031
[43] Dalrymple B J and Prober D E 1984 *J. Low Temp. Phys.* **56** 545
[44] Rainer D and Bergmann G 1974 *J. Low Temp. Phys.* **14** 501
[45] Mattheiss L F and Testardi L R 1979 *Phys. Rev.* B **20** 2196
[46] Li J, Guo Y-F, Yang Z-R, Yamaura K, Takayama-Muromachi E, Wang H-B and Wu P-H 2016 *Supercond. Sci. Technol.* **29** 053001
[47] Chubukov A V, Efremov D and Eremin I 2008 *Phys. Rev.* B **78** 134512
Parker D, Dolgov O V, Korshunov M M, Golubov A A and Mazin I I 2008 *Phys. Rev.* B **78** 134524
Mishra V, Boyd G R, Graser S, Maier T, Hirschfeld P J and Scalapino D J 2009 *Phys. Rev.* B **79** 094512
Senga Y and Kontani H 2009 *New J. Phys.* **11** 035005
[48] Ferrando V *et al* 2007 *J. Appl. Phys.* **101** 043903
[49] Nolscher C and Saemann-Ischenko G 1985 *Phys. Rev.* B **32** 1519
[50] Gurevich A 2003 *Phys. Rev.* B **67** 184515
[51] Dahm T and Schopohl N 2003 *Phys. Rev. Lett.* **91** 017001
[52] Martinelli A, Tarantini C, Lehmann E, Manfrinetti P, Palenzona A, Pallecchi I, Putti M and Ferdeghini C 2008 *Supercond. Sci. Technol.* **21** 012001
[53] Flükiger R *et al* 2017 *Supercond. Sci. Technol.* **30** 054003
[54] Testardi L R and Mattheiss L F 1978 *Phys. Rev. Lett.* **41** 1612
[55] Mentink M G T, Dhalle M M J, Dietderich D R, Godeke A, Hellman F and ten Kate H H J 2017 *Supercond. Sci. Technol.* **30** 025006
[56] Wiesmann H, Gurvitch M, Ghosh A K, Lutz H, Kammerer O F and Strongin M 1978 *Phys. Rev.* B **17** 122
[57] Putti M, Brotto P, Monni M, Galleani d' Agliano E, Sanna A and Massidda S 2007 *Europhys. Lett.* **77** 57005
[58] Putti M, Vaglio R and Rowell J M 2008 *Supercond. Sci. Technol.* **21** 043001
[59] Nekrasov I A, Pchelkina Z V and Sadovskii M V 2008 *JETP Lett.* **87** 560
[60] Schwingenschlögl U and Schuster C 2007 *Europhys. Lett.* **77** 37007
[61] Krasnosvobodtsev S I, Shabanova N P, Ekimov E V, Nozdrin V S and Pechen' E V 1995 *Zh. Eksp. Teor. Fiz.* **108** 970
Krasnosvobodtsev S I, Shabanova N P, Ekimov E V, Nozdrin V S and Pechen' E V 1995 *JETP* **81** 534
[62] Vonzovski S V, Izyumov Y A and Kurmaev E K 1982 *Superconductivity of Transition Metals* (Berlin: Springer)
[63] Liu A Y, Mazin I I and Kortus J 2001 *Phys. Rev. Lett.* **87** 087005
[64] Bouquet F, Fisher R A, Phillips N E, Hinks D G and Jorgensen J D 2001 *Phys. Rev. Lett.* **87** 047001
[65] Drechsler S-L *et al* 2008 *Phys. Rev. Lett.* **101** 257004
[66] Carbotte J P, Schachinger E and Basov D N 1999 *Nature* **401** 354
[67] Dagan Y, Krupke R and Deutscher G 2000 *Phys. Rev.* B **62** 146
[68] Pakokthom C, Krunavakarn B, Udomsamuthirun P and Yoksan S 1998 *J. Supercond.* **11** 429
[69] Chiao M, Hill R W, Lupien C, Taillefer L, Lambert P, Gagnon R and Fournier P 2000 *Phys. Rev.* B **62** 3554
[70] Robert Schrieffer J (ed) 2007 *Handbook of High-Temperature Superconductivity: Theory and Experiment* (Berlin: Springer)
[71] Singh D J and Du M-H 2008 *Phys. Rev. Lett.* **100** 237003

[72] Perucchi A *et al* 2010 *Phys. Rev.* B **81** 092509
[73] Tolpygo S K, Lin J-Y, Gurvitch M, Hou S Y and Phillips J M 1996 *Phys. Rev.* B **53** 12454
[74] Pallecchi I, Bernardini F, Caglieris F, Palenzona A, Massidda S and Putti M 2013 *Eur. Phys. J.* B **86** 338
[75] Ekino T, Takasaki T, Muranaka T, Akimitsu J and Fujii H 2003 *Phys. Rev.* B **67** 094504
[76] Rullier-Albenque F, Alloul H and Tourbot R 2003 *Phys. Rev. Lett.* **91** 047001
[77] Nakajima Y, Taen T, Tsuchiya Y, Tamegai T, Kitamura H and Murakami T 2010 *Phys. Rev.* B **82** 220504(R)
[78] Eisterer M, Zehetmayer M, Weber H W, Jiang J, Weiss J D, Yamamoto A and Hellstrom E E 2009 *Supercond. Sci. Technol.* **22** 095011
[79] Weaver B D 2014 *Physica* C **501** 36
[80] Nakajima Y, Tsuchiya Y, Taen T, Tamegai T, Kitamura H and Murakami T 2011 *Physica* C **471** 647
[81] Taen T, Ohtake F, Akiyama H, Inoue H, Sun Y, Pyon S, Tamegai T and Kitamura H 2013 *Phys. Rev.* B **88** 224514
[82] Blokin I S, Gavrilkin S Y, Dravin V A, Ivanenko O M, Krasnosvobodtsev S I, Mitsen K V and Tsvetkov A Y 2016 *J. Supercond. Nov. Magn.* **29** 1085–8
[83] Onari S and Kontani H 2009 *Phys. Rev. Lett.* **103** 177001
[84] Bang Y and Stewart G R 2017 *J. Phys. Condens. Matter* **29** 123003
[85] Korshunov M M, Togushova Y N and Dolgov O V 2016 *Phys.-Usp.* **59** 1211–40
[86] Hirschfeld P J and Physique C R 2016 *Comptes Rendus Phys.* **17** 197
[87] Gordon R T, Kim H, Tanatar M A, Prozorov R and Kogan V G 2010 *Phys. Rev.* B **81** 180501
[88] Li G, Hu W Z, Dong J, Li Z, Zheng P, Chen G F, Luo J L and Wang N L 2008 *Phys. Rev. Lett.* **101** 107004
[89] Drew A J *et al* 2008 *Phys. Rev. Lett.* **101** 097010
[90] Guo Y F *et al* 2012 *Phys. Rev.* B **85** 214509
[91] Daghero D, Tortello M, Gozzelino L, Gonnelli R S, Hatano T, Kawaguchi T and Ikuta H 2017 *Appl. Surf. Sci.* **395** 9
[92] Smylie M P *et al* 2016 *Phys. Rev.* B **93** 115119
[93] Blokhin I S, Gavrilkin S Y, Dravin V A, Ivanenko O M, Krasnosvobodtsev S I, Mitsen K V and Tsvetkov A Y 2016 *J. Supercond. Nov. Magn.* **29** 1085
[94] Cho K, Konczykowski M, Murphy J, Kim H, Tanatar M A, Straszheim W E, Shen B, Wen H H and Prozorov R 2014 *Phys. Rev.* B **90** 104514